Oxygen-defect characterization for improving R&D relevance and Cz-Si solar cell efficiency

Jordi Veirman, **Benoît Martel**, **Nicolas Enjalbert** & **Sébastien Dubois**, CEA Tech-INES, Le Bourget du Lac, & **Catherine Picoulet** & **Pierre Bonnard**, AET Technologies, Meylan, France

ABSTRACT

Most high-efficiency solar cells are fabricated from monocrystalline Czochralski (Cz) silicon (Si) wafers because of the high quality of the material. Despite the considerable heritage from microelectronics, the Cz-Si substrate quality can still limit cell performance. A key issue regarding wafer quality relates to the presence of oxygen in the bulk. Cz wafers indeed feature high oxygen concentrations owing to the silica crucible dissolution during crystal growth. Although not harmful as such, oxygen is a very reactive impurity that can form a plurality of recombination-active defects before, during, or after cell processing. It is now well known that the formation of these defects can lead to reductions in PV conversion efficiency of several per cent absolute. Furthermore, the formation/annihilation of these defects can interfere with cell process optimizations; it can also impact R&D activity or the integration/ramping up of new process tools in a production line. As a consequence, it is of paramount importance to both wafer and cell manufacturers that the Cz substrate quality be controlled. This paper introduces a characterization technique called *OxyMap*, which aims to provide a detailed analysis of oxygen and related defects in Cz-Si wafers. The capabilities of the OxyMap technique are presented and illustrated with the help of statistical data obtained for wafers and cells from the main PV players in the industry. Large variations in material quality are revealed among the tested wafers, highlighting the need for quality control in order to optimize the ingot yield/quality and to increase the cell efficiency/reliability.

Introduction

Solar cell structures labelled as 'high efficiency' (>20% in production) are mostly processed from high-quality Cz wafers. The main requirement for such Cz wafers is a long and spatially uniform charge-carrier lifetime (τ) that additionally does not degrade – neither during the cell process nor under outdoor operating conditions. While the first requirement ensures that optimum conversion efficiency is achieved, the second prevents any cell efficiency degradation and cell mismatch at the module level. Commercial Cz ingots, however, seldom meet these specifications from seed to tail (i.e. from top to bottom). Rather, a wide range of recombination-active defects originating from ingot growth can be present in the finished solar cell.

Defects can be classified into three categories, on the basis of whether they are activated during 1) crystal pulling, 2) cell processing, or eventually 3) cell operation. The vast majority of these defects are related to the presence of oxygen in the crystal lattice. Oxygen is incorporated in interstitial positions (O_i) into the ingot in concentrations in the range 6–25ppma, following the dissolution of the silica crucible in the Si melt. The main category 1 defects are oxygen-related thermal donors (TDs) [1], and complexes involving intrinsic point defects, such as vacancy-oxygen (V-O) [2]. Category 2 defects are mostly oxide precipitates and related extended defects, possibly decorated by metallic impurities [3] (may be category 1 defects if ingot crystallization is poor). Belonging to category 3 are those defects activated upon illumination of the cell, such as the well-known boron-oxygen (BO) complex in boron (B)-doped wafers [4], or other defects still under investigation in phosphorus (P) doped wafers [5].

To better illustrate the detrimental effect of oxygen, it is estimated that 10–20% of shipped wafers are affected by oxide precipitation when processed into 20–21% n-PASHA homojunction cells [6]. For amorphous/crystalline Si heterojunction cells processed on seed-end wafers, efficiency drops of around 1%$_{abs}$ were also reported [7], presumably because of TDs and/or oxide precipitates. Last, but not least, BO complexes particularly affect passivated emitter and rear cells (PERCs), thereby limiting their rate of entry into the market.

"It is imperative to develop ways of monitoring and mitigating the concentration of oxygen and related defects throughout the wafer."

In spite of the legacy handed down from microelectronics in the art of crystal pulling, the unprecedented τ specifications of high-efficiency cells call for further research and development. In particular, it is imperative to develop ways of monitoring and mitigating the concentration of oxygen and related defects throughout the wafer (unlike microelectronics wafers for which only the near surface – the so-called *denuded zone* – is used for device processing). They may otherwise be an early showstopper for the industry on the way towards achieving the 29.4% theoretical maximum efficiency [8]. In this context, AET Solar Tech and CEA-INES have developed a technique called *OxyMap* in the frame of the eponymous project. OxyMap provides a wide picture of oxygen-related defects in Cz wafers for R&D and quality-control purposes, and has now been implemented in a commercial tool. The fundamental features of the technique are detailed and the potential benefits for the PV community are discussed.

OxyMap measurement: step by step

The patented procedure relies on the change in resistivity (ρ) when the TD concentration ([TD]) in the wafer is modified in a controlled manner. ρ is defined as $(mq\mu)^{-1}$, where q is the elementary charge, and m and μ are the majority-carrier density and drift mobility respectively. TDs are thought

to be small O_i aggregates formed at temperatures in the range 350–600°C, and most effectively at 450°C. Owing to the very strong dependence of TD-formation kinetics and amplitude on the O_i concentration ($[O_i]$) [9], [TD] is usually insignificant in oxygen-lean float zone Si and multicrystalline Si. Conversely, it is readily generated in Cz-Si in concentrations of up to a few $10^{16}cm^{-3}$. Because it possesses a double-donor character for typical ρ in PV, its formation/annihilation leads to a measurable change in ρ, on which the OxyMap technique is based.

The procedure consists of two anneal steps, with a ρ measurement before and after each anneal (named chronologically ρ_1, ρ_2 and ρ_3). The first heat treatment is carried out at 450°C for two to three hours, with the aim of generating TDs ($[TD]_{450}$) in sufficient numbers to induce a measurable change in ρ. The second treatment is performed above 700°C for a few minutes, leading to TD annihilation. From this set of ρ data, typically obtained from a four-point probe or non-contact eddy current measurements, a wide set of output values can be calculated. An overview of the full procedure is given in Fig. 1. The calculation details are presented hereafter for p-type B-doped wafers. In the case of n-type P-doped wafers, the B concentration ([B]) ought to be replaced by that of P ([P]), and the minus sign by a plus; the mobility term should be that corresponding to majority electrons (μ_e).

Prior to any intentional thermal treatment, when ρ_1 is measured, the wafer contains a certain number of TDs formed during crystal cooling ($[TD]_{ini}$), which compensates for the intentional acceptor doping provided by B atoms. After the 450°C anneal, when ρ_2 is measured, the concentration of intentionally formed TDs ($[TD]_{450}$) further adds up to the already existing $[TD]_{ini}$. Following the 700°C heat treatment, when ρ_3 is measured, the wafer is eventually left TD free and therefore contains virtually only B as doping species. ρ_1, ρ_2 and ρ_3 are thus expressed using the following set of equations, where $\mu_{h,n}$ (n=1, 2, 3) is the majority hole drift mobility and depends on the concentrations of all doping species [10]:

$$\rho_1 = \frac{1}{([B] - 2\times[TD]_{ini})\times q \times \mu_{h,1}} \quad (1)$$

$$\rho_2 = \frac{1}{([B] - 2\times([TD]_{ini} + [TD]_{450}))\times q \times \mu_{h,2}} \quad (2)$$

$$\rho_3 = \frac{1}{[B]\times q \times \mu_{h,3}} \quad (3)$$

The factor 2 arises from the predominance of the doubly ionized state of TD in usual PV materials [11,12]. To capture the recently discovered effect of compensation on μ, the enhancement of Klaassen's model as proposed by Schindler et al. [13] is used. Note that $\rho_3 < \rho_1 < \rho_2$ in p-type Si, and $\rho_3 > \rho_1 > \rho_2$ in n-type Si, which allows the conductivity type to be determined. The next steps essentially involve solving Equations 1–3 for the three unknowns [B], $[TD]_{ini}$ and $[TD]_{450}$: once [B] has been determined from Equation 3, the value of $[TD]_{ini}$ is extracted using Equation 1, and $[TD]_{450}$ is eventually worked out from Equation 2.

$[O_i]$ is subsequently determined using an internally developed empirical expression for the TD generation kinetics at 450°C. This expression was established from a set of 42 samples prepared from the bottom, middle and top sections of industrial-like ingots. These 3mm-thick slices included both p- and n-type material, from a wide range of ρ (from 0.5 to 200Ω·cm). The samples were mirror-polished to allow $[O_i]$ measurements by Fourier transform infrared (FTIR) spectroscopy, routinely used in industry for $[O_i]$ measurements. Note that the FTIR analyses reported throughout this paper were performed in accordance with the SEMI-recommended ASTM F1188-93a associated with the IOC88 calibration coefficient of 6.28ppma·cm. The $[O_i]$ values provided by OxyMap, which is an FTIR-calibrated technique, are also given with respect to ASTM F1188-93a. Historically, however, the prevailing norm in the industry has been ASTM F121-83, associated with the DIN coefficient of 4.9ppma·cm. This leads to a 22% difference in derived $[O_i]$ between the two norms. It should be stressed that in order to allow relevant comparisons between the two, the appropriate conversions must be made.

"The strong dependence of TD formation on $[O_i]$ gives the OxyMap technique its outstanding sensitivity."

The evolution of $[TD]_{450}$ with annealing time was then accurately monitored on the same samples using four-point probe ρ measurements and Equations 1 to 3. It was confirmed that TD-formation kinetics depend very strongly on $[O_i]$; by way of example, the TD formation rate is accelerated by a factor of 170 with just a fourfold increase in $[O_i]$ (from 6 to 25ppma). This outstanding sensitivity property of TDs is imparted to the OxyMap technique: the strong dependence of TD formation on $[O_i]$ gives the OxyMap technique its outstanding sensitivity.

The kinetic model $[TD]_{450} = f([O_i],t)$ was then used in the OxyMap technique to allow the conversion of $[TD]_{450}$ into $[O_i]$ data. The agreement achieved between OxyMap and FTIR measurements was within 5% (see Fig. 2). Note that a departure from the black curve ($x = y$) in Fig. 2 would be expected in the presence of excessive column IV elements. For a given $[O_i]$, these elements are indeed known to slow down the TD-formation kinetics; among them, carbon is typically encountered in Cz crystals because of graphite elements. Nevertheless, the threshold carbon content above which this slowing-down occurs is around 2ppma, which exceeds usual specifications.

In the next step, the accuracy of the OxyMap $[O_i]$ measured for thin as-cut wafers (<200µm) was put to the test, by a comparison with the FTIR values obtained for neighbouring thick polished slices. Some representative examples are shown for both n- and p-type Si in Fig. 3. In these cases, the OxyMap

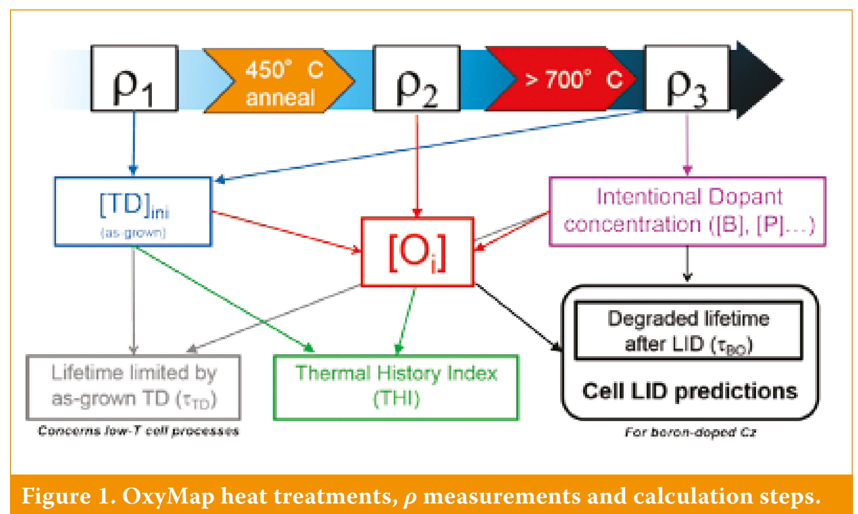

Figure 1. OxyMap heat treatments, ρ measurements and calculation steps.

technique was performed on wafers regularly sampled along 8" industrial ingots, using a non-contact eddy current head for the ρ measurements. The overall agreement achieved is excellent. When OxyMap is used on thin as-cut wafers for $[O_i]$ measurements rather than FTIR, thick polished slices are no longer required and can be turned into wafers instead, thereby enabling significant savings.

As a result of random scattering of the infrared beam at the surfaces and chaotic internal multireflections, standard FTIR is not really applicable to thin as-cut wafers. An elegant upgrade of the FTIR technique was recently suggested to solve this issue [14], but it is destructive and requires very careful sample cleavage. OxyMap, on the other hand, has been shown to perform equally well whatever the thickness – at least down to a thickness of 80µm [11].

If ρ_1, ρ_2 and ρ_3 measurements are now performed in the form of a line scan along the wafer diagonal, and taking into account the quasi-centrosymmetric defect distribution in Cz wafers inherent to the process itself, OxyMap can provide each output value from Fig. 1 in the form of a 2D mapping. An example of an $[O_i]$ mapping is given in Fig. 4: the usual hill-shaped $[O_i]$ profile is revealed, which results from convection-induced piling-up of O in the melt under the crystal centre. Typical slight radial oscillations in $[O_i]$ due to growth rate fluctuations can also be observed.

Since the OxyMap procedure involves high-temperature treatments likely to modify the wafer properties significantly, it was considered relevant to assess whether measured wafers could be reused as substrates for high-efficiency device manufacturing. For Al-BSF cells processed by third parties (efficiency >19%), no systematic change in efficiency was observed, compared with cells processed from reference wafers (i.e. not measured with OxyMap). In the worst-case experiment, a $0.2\%_{abs}$ average reduction was observed, which may be attributed to contamination caused by additional handling of wafers. In the case of heterojunction cells, different behaviours were observed, depending on wafer providers, with even slight gains noticed for some of them, presumably from the benefits of the >700°C temperature step. More data should however be collected before drawing conclusions.

All the features in Fig. 1 have been implemented in an R&D tool commercialized by AET Technologies. Metrology characteristics were estimated for this tool. The wafer-to-wafer repeatability on $[O_i]$ turned out to be better than 2%, while the resolution (smallest detectable variation in $[O_i]$) was around 0.3ppma. The measurement accuracy associated with $[O_i]$ is mainly driven by uncertainties in the ρ measurements. The closer together ρ_1 and ρ_2 are, the larger the uncertainties become. The worst-case scenario thus concerns low ρ_1 and O_i-lean p-type wafers. If one considers, for instance, a B-doped 1Ω·cm with $[O_i]$ = 10ppma, an uncertainty of ±20% is expected (including the aforementioned ±5% – see Fig. 2); however, this rapidly shrinks to ±5% as either $[O_i]$ increases or the doping decreases. For pulling-process optimizations, it is recommended that measurements of low $[O_i]$ be performed on lightly doped ingots. In principle, $[O_i]$ as low as 6ppma can be measured with a ±7% accuracy for a 5Ω·cm n-type material.

Cell LID predictions

Since the early days of the OxyMap technique [10], several new features have been gradually introduced. Because the technique allows both [B] and $[O_i]$ to be determined, it was decided to trust the technique further and assess its capability to predict from as-cut wafers the light-induced degradation (LID) related to the BO complex in B-doped cells.

In a first step, the carrier lifetime limited by the formation of the BO complexes after LID (τ_{BO}) at an excess carrier density (Δn) equal to [B]/10 was predicted using the OxyMap [B] and

Advanced characterization technology to qualify Cz Silicon wafers & ingots

Large set of accurate data dedicated to:
- material qualification and sorting for Cz wafer suppliers/users
- optimization of ingots and cells manufacturing processes

Thickness independent

Operator independent

Non destructive

No sample preparation

Reproducible

No restriction on wafer surface roughness

No material loss

No restriction on wafer thickness

+33 (0)4 76 904 118
http://aetsolartech.com/

AUVERGNE – RhôneAlpes

[O_i] values. To this end, the well-known empirical expression from Bothe et al. [4] was used:

$$\tau_{BO} = a \times 7.675 \times 10^{45} \times [B]^{-0.824} \times [O_i]^{-1.748} \quad (4)$$

The beneficial effect of the P emitter formation on the LID amplitude is taken into consideration here by setting a to 2, as reported in Bothe et al. [4]. The validity of the τ_{BO} predictions was experimentally verified by comparison with the τ_{BO} measured for diffused and then emitter-etched wafers from 10 different providers [15].

Following this preliminary verification, algorithms describing the relative LID loss for each PV parameter were established [15,16] for a wide range of realistic τ_{BO} values (i.e. of [B] and [O_i]). For this purpose, the PC1D software was used; τ_{BO} and its variation with Δn were modelled with the recombination parameters from Rein et al. [17]. The first simulations were run for a 180µm-thick Al-BSF cell with a pre-LID efficiency of 18.5%. Experimentally measured values were used as input parameters for the diffused emitter ([P] profile), the Si nitride coating (spectral variation of the reflectance and front-surface recombination velocity), and the screen-printed metallization (series and shunt resistances). For the back-side Al-BSF, an approximated Al concentration profile and rear-surface recombination velocity were used, as they were not known accurately at that time. The relative losses computed for each PV parameter were plotted as a function of both [B] and [O_i]. They were then successfully fitted using exponential-like expressions – with [B] and [O_i] as the only variables – and further fine-tuned to reproduce the measured losses for 18.5% Al-BSF CEA cells (mainly in order to include small differences between the simulated and the experimental structures).

The LID prediction algorithms were extensively tested with third parties in the framework of the project. As an example, Fig. 5 shows a comparison of predicted and measured LID losses (0.1W.cm^{-2} illumination for 48h at 25°C) for 19.5% (pre-LID) Al-BSF cells. The devices were processed at a partner's site on wafers from three providers. The losses in efficiency span a wide range of values, from around 1 to 3%$_{rel}$, revealing large variations in material quality. A fairly good agreement between predictions and measurements was obtained. The observed scattering – typical for such comparisons – can have multiple root causes: it can result from cumulative uncertainties in the LID losses measurements, in the cell and software models, and in the [O_i] and [B] measurements.

Because of the significant differences in efficiency between the cells used for establishing the semi-empirical model and the processed cells, the agreement achieved may initially appear questionable. Indeed, one would expect significantly larger relative LID losses for the 19.5%-efficient processed cells, because of the greater sensitivity to τ. However, the 19.5% cell operates at a higher Δn, where the τ limited by the BO complexes is higher (owing to their asymmetric electron- and hole-capture cross sections). Simulations show that this injection-level effect maintains a reasonable LID amplitude

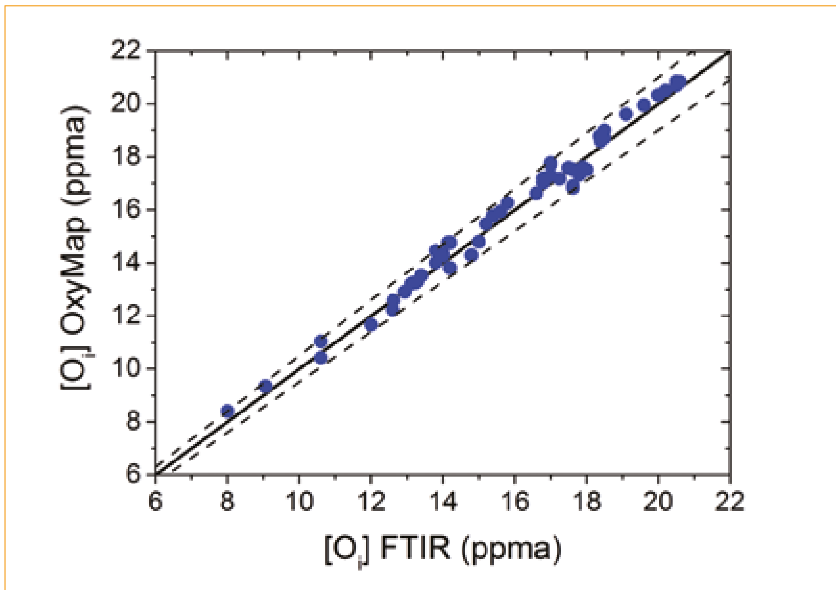

Figure 2. Agreement between OxyMap and FTIR measurements for the set of 42 thick polished wafers. (The dashed lines indicate variations of ±5%.)v

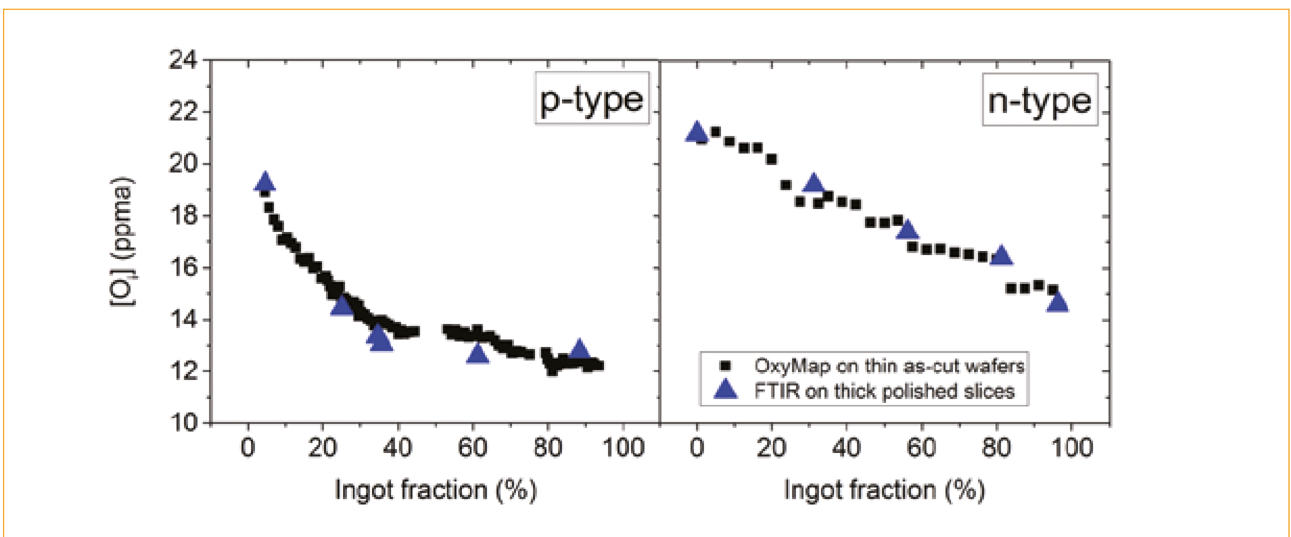

Figure 3. [O_i] profiles measured using OxyMap on 180µm-thick as-cut wafers (squares) and 2mm-thick mirror-polished slices using FTIR (triangles).

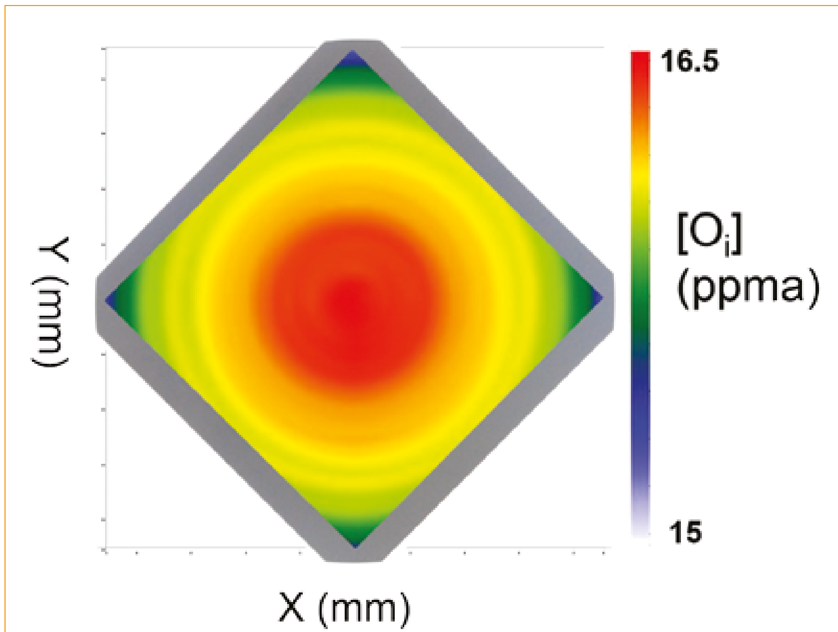

Figure 4. Example of an $[O_i]$ mapping. Such mappings can be computed for all output values listed in Fig. 1.

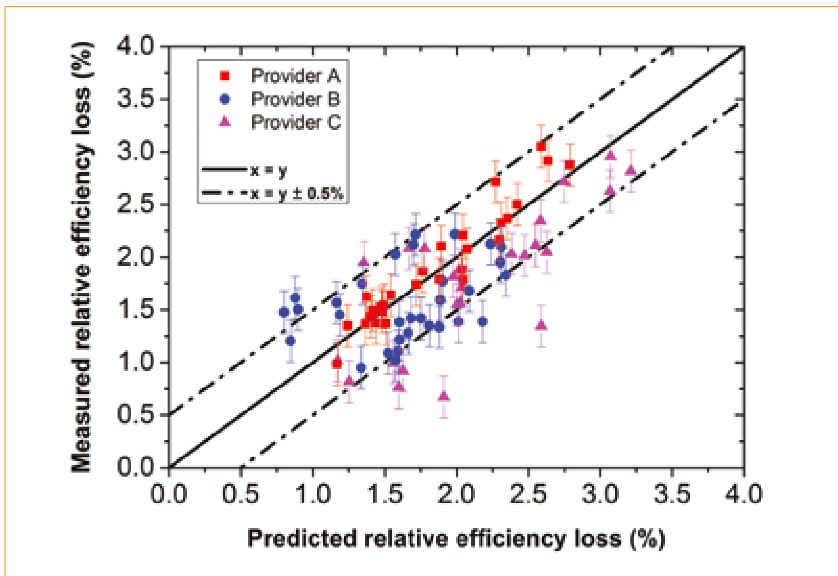

Figure 5. Comparison of predicted and experimental LID losses for three sets of cells.

for 19.5%-efficient devices – only slightly more than that for the 18.5% simulated cell (typically 10–15%$_{rel}$ higher amplitudes [18]). Such a slight deviation would be hardly detectable in practice because of the aforementioned data scattering, as revealed in Fig. 5.

It is known that the cell architecture and its fabrication process can influence the LID losses [18,19]. To take this into account, the OxyMap tool from AET Technologies also allows the user to enter home-made LID prediction algorithms based on OxyMap $[O_i]$ and [B] values. This alternative is particularly attractive for PERC cells (usually highly sensitive to LID), whose comparatively recent adoption by the industry leads to a larger variety of existing processes, making it unlikely that a universal PERC-LID model could be achieved.

It is believed that the LID predictions can be of great help to cell manufacturers in order to benchmark wafers providers, or for the ramping-up of anti-LID processes, such as the new light-induced regeneration tools. Performing these predictions at the wafer level means that any cell processing or time-consuming ageing tests are avoided.

Detection of poor-quality wafers

For R&D needs, sheet resistance (R_{sheet}) of highly doped surfaces and implied open-circuit voltage (i-V_{oc}) are routinely measured in order to optimize cell processes. Both R_{sheet} and i-V_{oc} measurements depend heavily on the wafer ρ which is traditionally measured on as-cut wafers prior to any processing. It is generally assumed that ρ is stable throughout the cell processing sequence; however, large ρ variations can be expected after >650°C anneals (owing to TD_{ini} dissolution), making this assumption questionable. Fig. 6, based on the statistics for ~1,400 wafers of both types from 15 industrial providers, reveals that around 20% of the tested wafers feature a ρ variation after >650°C anneals greater than 10% and up to 200%, which can invalidate R_{sheet} and i-V_{oc} values. It is roughly estimated, for instance, that a 50% unexpected ρ variation can lead to biases of around 10% in R_{sheet} for a standard P emitter, and of 5mV in i-V_{oc} for an i-V_{oc} of ~680mV (with, of course, worse results for larger variations in ρ). The identification of wafers with a stable ρ (or the knowledge of ρ after high-temperature steps) using OxyMap is therefore an asset for improving the accuracy of R&D data.

> "The identification of wafers with a stable ρ using OxyMap is an asset for improving the accuracy of R&D data."

For production purposes, OxyMap can help identify poor-quality wafers, which will result in lower efficiency. Except perhaps in case of excessive contamination by metallic elements, many lifetime-limiting defects are related to O_i in Cz-Si. Nevertheless, a tentative identification of poor wafers based solely on $[O_i]$ is prone to failure. Indeed, other parameters (such as the thermal history) greatly influence the number of O-related defects. The thermal history is defined as the temperature vs. time profile that is experienced during crystal growth. Since a typical pulling process lasts for several tens of hours, seed-end wafers feature a much longer thermal history than tail-end wafers, the latter being crystallized last; for a given $[O_i]$, they are therefore more likely to contain O-related defects. It is well known, for instance, that TDs form preferentially at the ingot seed-ends, where the material experiences the longest time within the TD-formation temperature range.

In order to improve the capacity of OxyMap to detect poor-quality wafers, $[O_i]$ was tentatively combined with a thermal history index (THI, in minutes) in order to establish a novel wafer quality indicator [20]. The THI was calculated from the measured values of $[O_i]$ – the

'driving force' for TD formation – and $[TD]_{ini}$, the 'relic' that results from the expression of this driving force during the crystal cooling.

Fig. 7 depicts an example of 156 PSQ n-PERT (passivated emitter, rear totally diffused) solar cells processed at CEA-INES; with the process used at the time of this study, the baseline efficiency was around 20% [21]. Wafers were sampled from two commercial ingots from the same manufacturer. While both ingots feature similar THI profiles, $[O_i]$ peaks at different locations: in Ingot 1, $[O_i]$ peaks at the point where THI is high, whereas in Ingot 2, $[O_i]$ peaks at the point of low THI. As represented by the solid rectangle, large $[O_i]$ in conjunction with large THI wafers were associated with decreased efficiencies. The corresponding PERT cells showed a low hole-diffusion length core at the cell centre, which is usually related to oxide precipitates [22,23]. On the other hand, the occurrence alone of a high THI or a high $[O_i]$ (dashed green rectangles) did not lead to any efficiency reductions. It is therefore concluded that $[O_i]$ in combination with THI can be used as a quality indicator to detect wafers affected by O-related issues. Note that similar conclusions have been drawn for rear-emitter heterojunction solar cells [20]. For a given cell process, a maximum acceptable threshold value for the combination can thus be set for rejecting poor-quality wafers and for improving the overall cell efficiency of the production line.

It should be stressed here that, because Si vacancies can play an important role in oxygen precipitation [24], the correlation between $[O_i]$, THI and bulk-related efficiency reductions might not be systematic. Future studies involving a larger number of ingots/cell processes should help in specifying, for the different processes, the significance and threshold values for the '$[O_i]$+THI' indicator.

Feedback for pulling-process optimizations

A mapping of the THI at the ingot level can be reconstructed from a set of 2D wafer mappings; an example of such an ingot mapping is shown in Fig. 8. In this example, a region with a high THI of around 500min is evidenced close to the seed-end, which suggests a slow cooling after crystallization, thereby promoting O-related defect formation. Such feedback can in turn be used to drive advances in R&D. The benefits of a new hot-zone design can be directly assessed, for instance, by its effect on the THI distribution. Note that, by definition, the THI is representative of the length of time spent in the TD-formation range (i.e. 600–350°C) during cooling down. It is tacitly assumed here by extension that it is also representative of the overall cooling profile. Simulation tasks are ongoing at CEA-INES in order to assess the validity of this assumption for today's industrial pulling processes.

Similar mappings can be reconstructed for all parameters in Fig. 1, such as $[O_i]$. Spatial variations, as well as the absolute $[O_i]$, are largely determined by crystal growth parameters [1]. In an attempt to lower $[O_i]$ and its radial variations, R&D teams can therefore benefit greatly from such characterizations in terms of accelerating crystallization process improvements.

Influence of thermal donors on the electrical properties

In addition to their well-known dopant character, TDs can induce a significant recombination activity. Heterojunction cells are fabricated using low-temperature processes (generally <250°C) that do not annihilate TD_{ini}, unless a specific thermal donor anneal is performed beforehand. TD_{ini} can in turn induce efficiency reductions of up to $4\%_{abs}$, for values encountered in commercial ingots (i.e. from a few $10^{13}cm^{-3}$ up to $2\times10^{15}cm^{-3}$, according to our database) [25]. When the model developed by our group in Tomassini et al. [25] is used, the lifetime limited by TD_{ini} (τ_{TD}) can be calculated from OxyMap data and subsequently mapped across the wafer. Such a mapping can be obtained directly from OxyMap measurements for as-cut wafers, i.e. without the need for surface passivation.

In order to check the mapping validity, wafers containing TDs ($[TD]_{ini}$ ~$1.9\times10^{15}cm^{-3}$) were measured by OxyMap to yield 2D mappings of τ_{TD}; meanwhile the sister wafers were etched and cleaned before passivation of both surfaces using intrinsic and n-type amorphous Si stacks. The effective carrier lifetimes of the passivated wafers were subsequently mapped from the photoconductance decay detected by microwave. A typical comparison of both types of mappings is given in Fig. 9. A very good qualitative agreement was achieved, illustrating the possibility of predicting the lifetime from OxyMap measurements of as-cut wafers.

Conclusion

The OxyMap technique, with the goal of providing an in-depth characterization of oxygen-related defects in Cz-Si, was developed step by step in the framework of the eponymous project. The technology has now matured and offers

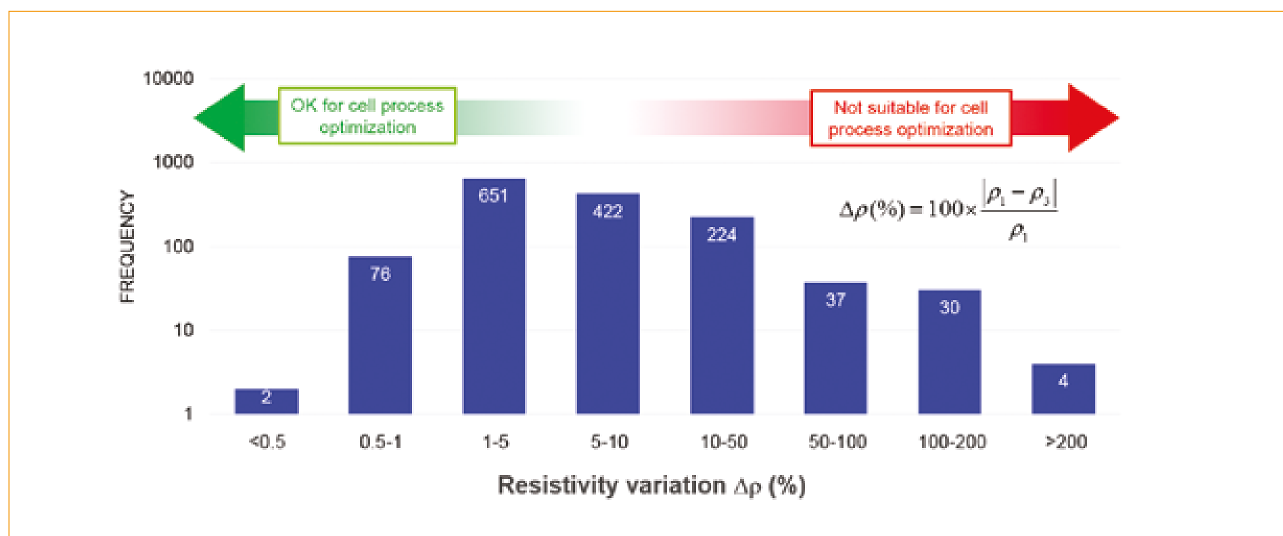

Figure 6. Relative variation in resistivity before/after a high-temperature step, measured by OxyMap. (Statistics for ~1,400 wafers from 15 industrial providers.)

a full range of features to the benefit of the PV community. All the presented features are now included in an R&D tool commercialized by AET Technologies.

It was shown that both ingot/wafer and cell providers can leverage the OxyMap output values to continually improve ingot quality and cell efficiency. The technique, which does not require any wafer preparation, is shown to be independent of the wafer thickness (down to thicknesses below 100µm), which makes it compatible with the expected trends of the PV industry. The OxyMap tool developed on this basis is operator independent and features batch-processing capabilities. It is believed that the tool represents a key opportunity for the PV industry to better characterize incoming/outgoing materials, and speed up the race towards higher-efficiency and more cost-effective solar cells, with attractive returns on investment.

> "It is believed that the OxyMap tool represents a key opportunity for the PV industry to better characterize incoming/outgoing materials."

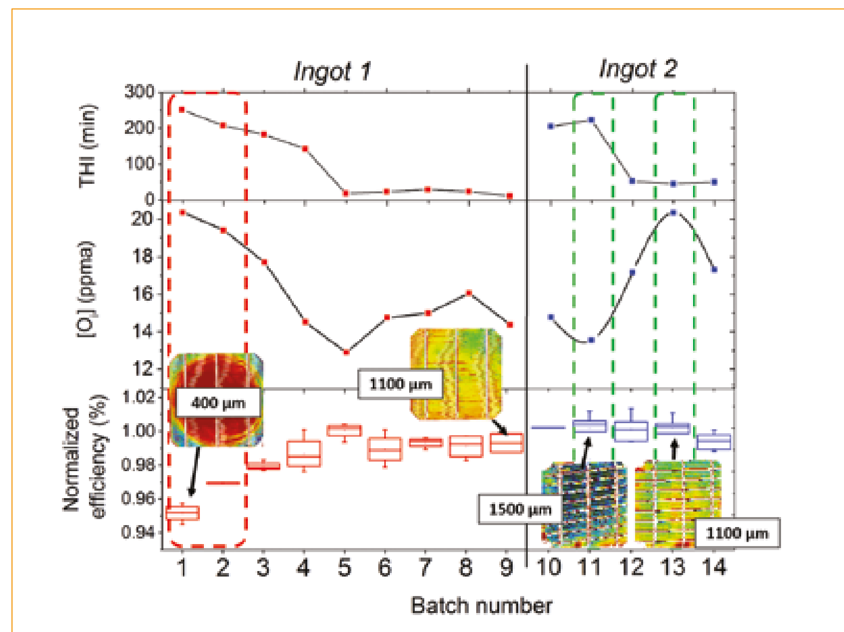

Figure 7. Comparison of n-PERT normalized cell efficiency with diagonal averaged [Oi] and THI for two Cz ingots. Hole-diffusion length mappings obtained from light-beam-induced current measurements are also shown (scale from 400 to 2000µm). The central hole-diffusion length values are given.

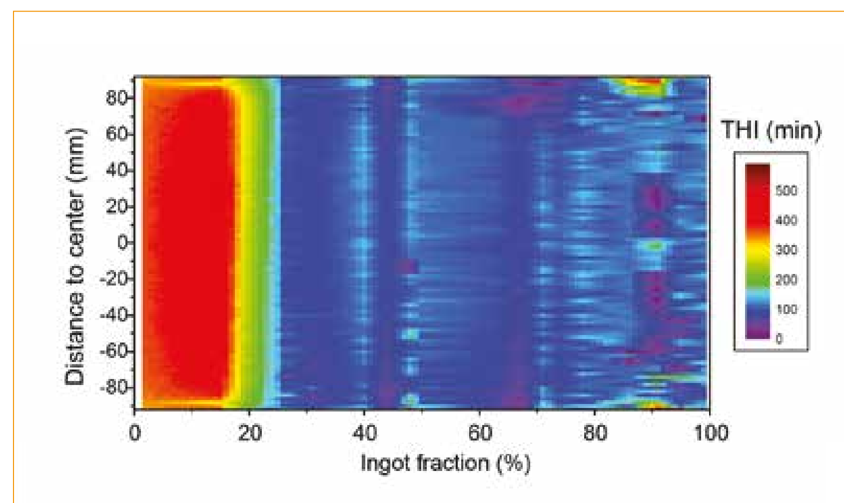

Figure 8. Example of a THI mapping of a 90kg 8" ingot, showing a region with extended cooling time (in red). (Reconstructed from 25 wafers measured using OxyMap.)

Acknowledgments

The CEA-INES and AET Technologies teams are indebted to Gintech, Hanwha Q CELLS, Norsun SA, Photowatt, FC3S group/CRPS/Air Liquide, ISC Konstanz, and other companies for feedback on the accuracy of OxyMap and/or for cell LID assessment.

Materials

References

[1] Shimura, F. (Ed.) 1994, *Oxygen in Silicon*. Boston: Academic Press, pp. 251–280.

[2] Zheng, P et al. 2014, "Evidence for vacancy-related recombination active defects in as-grown n-type Czochralski silicon", *IEEE J. Photovolt.*, Vol. 5, pp. 183–188.

[3] Murphy, J.D. et al. 2015, "The effect of oxide precipitates on minority carrier lifetime in n-type silicon", *J. Appl. Phys.*, Vol. 118, p. 215706.

[4] Bothe, K. et al. 2005, "Fundamental boron–oxygen-related carrier lifetime limit in mono- and multicrystalline silicon", *Prog. Photovoltaics Res. Appl.*, Vol. 13, pp. 287–296.

[5] Letty, E. et al. 2016, "Evidence of coexisting lifetime-limiting defects in as-received seed-end Czochralski wafers – Effect of light soaking", Presented at E-MRS spring meeting, Lille, France.

[6] Bronsveld, P.C.P. et al. 2015, "The effect of n-Pasha processing on bulk wafer quality", *Proc. 31st EU PVSEC*, Hamburg, Germany.

[7] Danel, A. et al. 2015, "Recent progress on the CEA-INES heterojunction solar cell pilot line", *Proc. 31st EU PVSEC*, Hamburg, Germany.

[8] Richter, A. et al. 2013, "Reassessment of the limiting efficiency for crystalline silicon solar cells", *IEEE J. Photovolt.*, Vol. 3, No. 4, pp. 1184–1191.

[9] Londos, C.A. 1993, "Effect of oxygen concentration on the kinetics of thermal donor formation in silicon at temperatures between 350 and 500°C", *Appl. Phys. Lett.*, Vol. 62, pp. 1525–1526.

[10] Veirman, J. et al. 2011, "A fast and easily implemented method for interstitial oxygen concentration mapping through the activation of thermal donors in silicon", *Energy Procedia*, Vol. 8, pp. 41–46.

[11] Veirman, J. 2012, "Oxygen mappings in silicon: From ultra-thin wafers to ingots", *Proc. 6th CssC*, Aix-Les-Bains, France.

[12] Voronkov, V.V. 2009, "Advanced application of resistivity and Hall effect measurements to characterization of silicon", *ECS Trans.*, Vol. 25, No. 3, pp. 25–34.

[13] Schindler, F. et al. 2014, "Towards a unified low-field model for carrier mobilities in crystalline silicon", *Sol.*

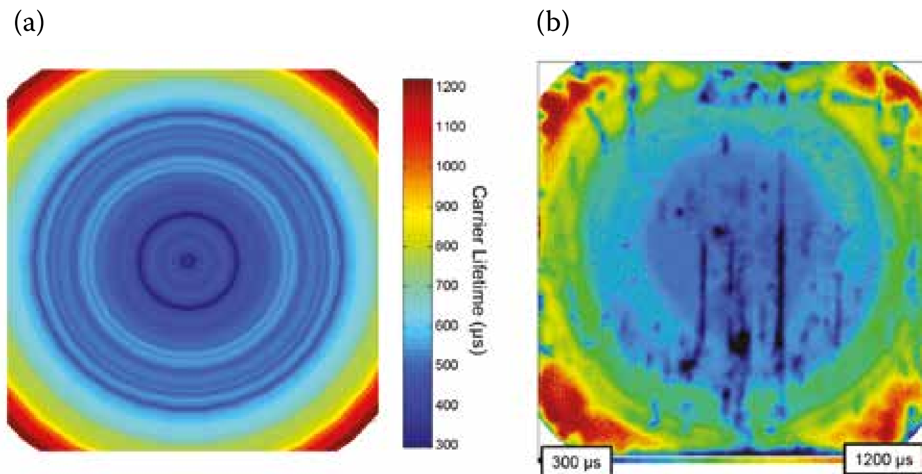

Figure 9. Typical comparison of effective carrier lifetimes: (a) OxyMap predicted (τ_{TD}); (b) measured.

Energy Mater. Sol. Cells, Vol. 131, pp. 92–99.

[14] Wolny, F. 2016, *Energy Procedia* [forthcoming].

[15] Veirman, J. et al. 2013, "Mapping of oxygen-related defects in silicon for high efficiency solar cells: Application to the prediction of LID losses", *Proc. 28th EU PVSEC*, Paris, France.

[16] Cascant, M. et al. 2014, "Investigating the spatial distribution of oxygen-related defects in Czochralski silicon wafers and ingots", *Proc. 8th SNEC*, Shanghai, China.

[17] Rein, S. et al. 2003, "Electronic properties of the metastable defect in boron-doped Czochralski silicon: Unambiguous determination by advanced lifetime spectroscopy", *Appl. Phys. Lett.,* Vol. 82, p. 1054.

[18] Das, A. 2012, "Development of high-efficiency boron diffused silicon solar cells", Ph.D. dissertation, Georgia Institute of Technology, Atlanta, USA.

[19] Altermatt, P. et al. 2009, "Highly predictive modelling of entire solar cells for industrial applications", *Proc. 24th EU PVSEC*, Hamburg, Germany.

[20] Veirman, J. et al. 2016 "Thermal history index as a bulk quality indicator for Czochralski solar wafers", *Sol. Energy Mater. Sol. Cells* [forthcoming].

[21] Cabal, R. et al. 2014, "20% PERT technology adapted to n-type mono-like silicon: Simplified process and narrowed cell efficiency distribution, *Proc. 29th EU PVSEC*, Amsterdam, The Netherlands.

[22] Letty, E. et al. 2016, "Identification of lifetime-limiting defects in as-received and heat treated seed-end Czochralski wafers", *Energy Procedia* [forthcoming].

[23] Haunschild, J. et al. 2012, "Cz-Si wafers in solar cell production: Efficiency-limiting defects and material quality control", *Photovoltaics International*, 15th edn, pp. 40–46.

[24] Falster, R. et al. 2000, "On the properties of the intrinsic point defects in silicon: A perspective from crystal growth and wafer processing", *physica status solidi (b)*, Vol. 222, p. 219.

[25] Tomassini, M. et al. 2016, "Recombination activity associated with thermal donor generation in monocrystalline silicon and effect on the conversion efficiency of heterojunction solar cells", *J. Appl. Phys.,* Vol. 119, p. 084508.

About the Authors

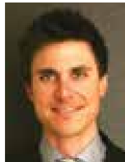

Jordi Veirman studied semiconductor physics at the National Institute for Applied Sciences (INSA) in Lyon, where he graduated with an engineering degree, followed by a master's in microelectronics in 2008. Since obtaining his Ph.D. from INSA, in the framework of which the foundations of the OxyMap technique were laid, he has been working as a project leader at CEA in the homojunction and heterojunction labs.

Benoît Martel started his career in the PV industry at PHOTOWATT as a cell process engineer. In 2011 he joined CEA-INES, to develop advanced characterization tools for PV applications. He is currently working as a research engineer and project leader on characterizing PV silicon defects and developing the cell process.

Nicolas Enjalbert started his career in the PV industry at PHOTOWATT, working on silicon wafers and cell characterizations. In 2005 he joined CEA-INES, where his research activities focus on solar-grade silicon, defects and advanced characterizations.

Sébastien Dubois studied materials science at the National Institute for Applied Sciences (INSA) in Lyon, and graduated with an engineering degree in 2004. In 2007 he received his Ph.D. in physics from Marseille University. After joining CEA-INES in 2007 he conducted and supervised research in the field of defects in crystalline silicon solar cells. He is currently responsible for the homojunction silicon solar cells laboratory.

Catherine Picoulet has been working at AET SolarTech since 2014. Among other activities, she is responsible for the business development and worldwide distribution of OxyMap technology. Prior to joining AET SolarTech, she held various senior positions as business development or operations manager at Applied Materials, Nextral and ASM.

Pierre Bonnard joined AET Technologies in 2005 after graduating with a master's in electrical specification from Grenoble Institute of Technology. He works on industrial furnaces as a senior electrical and automation engineer at AET Technologies, where he is also the product manager for the OxyMap tool.

Enquiries

Email jordi.veirman@cea.fr
cpicoulet@aet-technologies.fr